First Report of Bilateral External Auditory Canal Cochlin Aggregates ("Cochlinomas") with Multifocal Amyloid-Like Deposits, Associated with Sensorineural Hearing Loss and a Novel Genetic Variant in COCH Encoding Cochlin

DOI:
10.1007/s12105-019-01073-7

Document Version
Accepted author manuscript

Title page

Title: First report of bilateral external auditory canal cochlin aggregates ("cochlinomas") with multifocal amyloid-like deposits, associated with sensorineural hearing loss and a novel genetic variant in *COCH* encoding cochlin

Running head: Amyloid-like cochlin deposits in EACs

Precis: We present the first case of deafness associated with bilateral external auditory canal cochlin deposits, evidence suggestive of cochlin-derived amyloid formation, and a novel *COCH* variant. Our findings reveal a new pathologic manifestation of cochlin and highlight the importance of thoroughly investigating all aggregative tissue findings in the practice of diagnostic pathology.

Authors:

1. Atreyee Basu, MD (Department of Pathology, NYU) atreyee.basu@nyumc.org
2. Nicole J. Boczek, PhD (Department of Laboratory Medicine and Pathology, Mayo Clinic, Rochester, MN) Boczek.Nicole@mayo.edu
3. Nahid G. Robertson, PhD (Department of Obstetrics and Gynecology, Brigham and Women's Hospital, Boston, MA) nrobertson@research.bwh.harvard.edu
4. Samih H. Nasr, MD (Department of Laboratory Medicine and Pathology, Mayo Clinic, Rochester, MN) Nasr.Samih@mayo.edu
5. Daniel Jethanamest, MD (Department of Otolaryngology-Head and Neck Surgery, NYU) daniel.jethanamest@nyumc.org
6. Ellen D. McPhail, MD (Department of Laboratory Medicine and Pathology, Mayo Clinic, Rochester, MN) mcphail.ellen@mayo.edu
7. Paul J. Kurtin, MD (Department of Laboratory Medicine and Pathology, Mayo Clinic, Rochester, MN) kurtin.paul@mayo.edu
8. Surendra Dasari, PhD (Department of Health Sciences Research, Mayo Clinic, Rochester, MN) Dasari.Surendra@mayo.edu
9. Malinda Butz, BS (Department of Laboratory Medicine and Pathology, Mayo Clinic, Rochester, MN) Butz.Malinda@mayo.edu
10. Cynthia C. Morton, PhD (Departments of Obstetrics and Gynecology and of Pathology, Brigham and Women's Hospital, Harvard Medical School, Boston, MA; Broad Institute of MIT and Harvard, Cambridge, MA; University of Manchester, Manchester Academic Health Science Centre, Manchester, UK) cmorton@bwh.harvard.edu
11. W. Edward Highsmith, PhD* (Department of Laboratory Medicine and Pathology, Mayo Clinic, Rochester, MN) Highsmith.W@mayo.edu
    * in memoriam
12. Fang Zhou, MD (Department of Pathology, NYU) fang.zhou@nyu.edu

Corresponding author

Fang Zhou, MD

Address:

NYU Langone Hospital, Department of Pathology

560 First Avenue, TH 3-83

New York, N.Y. 10016

Email address: fang.zhou@nyu.edu

Telephone: 212-263-4895

Fax number: 212-263-7916

- Text pages: 10 (excluding the cover letter, title page, and figure legends)
- Number of tables: 0
- Numbers of figures: 7

Funding

C. C. Morton is supported by NIDCD R01DC015052 and the University of Manchester NIHR Biomedical Research Centre

Acknowledgments

We acknowledge Mayo Clinic Clinical Tissue Proteomics Laboratory for performing mass spectrometry experiments.

Conflict of interest

The authors declare that they have no conflict of interest.

Abstract (word count 248)

Pathogenic variants in *COCH*, encoding cochlin, cause DFNA9 deafness disorder with characteristic histopathologic findings of cochlin deposits in the inner and middle ears. Here, we present the first case of deafness associated with bilateral external auditory canal (EAC) cochlin deposits, previously unreported evidence suggestive of cochlin-derived amyloid formation, and a novel *COCH* variant.

A 54-year-old woman presented with progressive sensorineural hearing loss and bilateral EAC narrowing by subcutaneous thickening. Excision and histologic evaluation of tissue from both EACs showed paucicellular eosinophilic deposits containing multiple Congo red-positive foci with yellow and green birefringence under crossed polarization light microscopy. Mass spectrometry performed on both the Congo red-positive and Congo red-negative areas identified cochlin as the most abundant protein, as well as a low abundance of universal amyloid signature peptides only in the Congo red-positive areas. Peptides indicative of a canonical amyloid type were not detected. Electron microscopy showed haphazard, branched microfibrils (3-7 nm in diameter) consistent with cochlin, as well as swirling fibrils (10-24 nm in diameter) reminiscent of amyloid fibrils. Cochlin immunohistochemical staining showed positivity throughout the deposits. Sequencing of the entire *COCH* gene coding region from the patient's blood revealed a novel variant resulting in a non-conservative amino acid substitution of isoleucine to phenylalanine (c.1621A>T, p.I541F) in the vWFA2 domain in the protein's C-terminus.

Our findings reveal a new pathologic manifestation of cochlin, raise the possibility of previously undescribed cochlin-derived amyloid formation, and highlight the importance of thoroughly investigating all aggregative tissue findings in the practice of diagnostic pathology.

Keywords

Congo red; external ear canal stenosis; cochlin; amyloid; liquid chromatography tandem mass spectrometry; deafness

MANUSCRIPT

Introduction

Cochlin, the protein product of a deafness gene named coagulation factor C homology (*COCH*), is the most abundantly detected protein in the normal inner ear (cochlear and vestibular labyrinths) [1, 2]. Cochlin is also normally present in the middle ear interossicular joints and tympanic membrane pars tensa [3]. Pathogenic variants in *COCH* result in a distinct aggregative histopathology in these structures of the inner and middle ears [4, 5, 1, 6, 3]. To date, 29 distinct *COCH* mutations worldwide (Fig. 1) are known to cause DFNA9, an autosomal dominant disease consisting of progressive sensorineural hearing loss (SNHL) often accompanied by balance dysfunction. *COCH* is expressed at lower levels in normal cerebellum, eye, spleen, lung, brain, and thymus [7]. The protein is also found as aggregates in the trabecular meshwork of glaucomatous eyes in mice and human cadavers, but not in healthy eyes [8].

Cochlin is an extracellular protein consisting of the following domains (Fig. 1): coagulation factor C homology at the N-terminus (LCCL domain), which is thought to serve host defense functions, followed by two von Willebrand factor A-like domains (vWFA1 and vWFA2). vWFA domains are also present in a variety of other extracellular matrix (ECM) proteins, including several collagen types and cartilage matrix protein, and bind other proteins like fibrillar collagens, glycoproteins, and proteoglycans. Cochlin may serve a structural and tissue support role in the stabilization of the ECM. In addition, recent reports have elucidated an immune function of cochlin's LCCL domain, which has been associated with cytokine production, macrophage activation, and immune cell recruitment after exposure to pathogens, both systemically and locally in the inner ear compartment [9-11]. The dominant negative effects of *COCH* pathogenic variants are attributed to the gain of a deleterious function of cochlin, cochlin aggregation, and deposit formation. This is similar to other aggregative disorders such as Huntington disease (HD), wherein mechanisms of deposit formation result from gain-of-function due to gene alterations (*i.e.*, polyglutamine expansion in HD). The effects of *COCH* pathogenic variants on the immune and

inflammatory functions of cochlin are unknown, but nonetheless are likely not directly linked to the aggregative properties of cochlin.

In vitro studies have revealed that pathogenic variants in the LCCL domain can cause misfolding and multimerization of cochlin, and vWFA domain mutations can result in secretion failure and aggregate formation [12, 13]. In terms of DFNA9 histopathology as a result of *COCH* pathogenic variants, there are prominent eosinophilic acellular cochlin deposits and polymucosaccharide ground substance in the inner ear, which is the sensorineural portion of the auditory system [4, 5, 1]. There is remarkable loss of cellularity of the fibrocytes which express *COCH*, and downstream neuronal degeneration. Temporal bones from DFNA9 patients also exhibit both eosinophilic and basophilic aggregates in the conductive portion of the auditory system, depositing in the middle ear interossicular joints and causing thickening of the tympanic membrane [6, 3].

Here, we present the first report of Congo red-positive cochlin deposits in the external auditory canals (EACs) of a patient with SNHL (along with a family history of hearing loss), evidence suggesting amyloid formation by cochlin protein, and the presence of a novel *COCH* variant resulting in a non-conservative amino acid substitution.

Case description

A 54-year-old woman presented with progressive bilateral sensorineural hearing loss (SNHL). She had some high-frequency hearing loss since childhood and started wearing hearing aids in her early 30s. The patient's hearing did not improve with the use of a hearing aid or prednisone eardrops. In the last 7 years, she required frequent cerumen cleanings. She also had a family history of early-onset hearing loss in her brother, sister, and father. Her brother and father both had severe hearing loss starting in their 30s, while her sister only had mild high frequency hearing loss and did not wear any hearing aids. In addition, her brother and father both had glaucoma and the patient herself exhibited bilateral elevated intraocular pressures.

The patient went through an autoimmune workup, which revealed only an elevated anti-nuclear antibody (ANA). There was no other significant past medical or surgical history. Otomicroscopic examination revealed narrowing of both external auditory canals (EACs), left greater than right, with skin thickening but normal skin surface. Cerumen from the left EAC was removed. The remaining slit opening showed a limited view of the tympanic membrane (Fig. 2a). Cranial nerve examination was otherwise unremarkable and there were no other significant findings on physical examination.

An audiogram revealed mild sloping to profound SNHL in both ears. A computed tomography (CT) scan showed bilateral concentric soft tissue thickening of the EACs, without bony erosion. The stenosis involved the left EAC more so than the right, with nearly complete stenosis of the left EAC.

The patient underwent left meatoplasty and canaloplasty (Fig. 2b), followed by right meatoplasty and canaloplasty 16 months later. During both procedures, tan, gelatinous, semi-firm, subcutaneous soft tissue elements were identified in the cartilaginous EAC that appeared well-encapsulated grossly (Fig. 3a). As expected, the surgeries did not improve the patient's hearing loss because of its sensorineural nature. A conductive hearing loss component was not detected, but it may have been masked by the profound SNHL.

Methods

The specimens from both EACs were processed into formalin-fixed paraffin-embedded (FFPE) blocks at New York University Langone Hospital, where four-micron-thick sections were stained with hematoxylin and eosin (H&E), and eight-micron-thick sections were stained with Congo red using the Congo red staining kit and NexES Special Stains automated slide stainer from Ventana Medical Systems, Inc (Tucson, Arizona). At Mayo Clinic Laboratories in Rochester, MN, the Congo red stains were repeated and further characterization of the Congo red-positive material in each specimen was performed by liquid chromatography tandem mass spectrometry (LC-MS/MS)

[14]. Immunohistochemical staining of FFPE sections with an anti-cochlin antibody was performed as previously described, in the Morton Laboratory of Brigham and Women's Hospital [1]. A portion of the specimen from the right ear was placed in glutaraldehyde solution for transmission electron microscopy (TEM) at the Mayo Clinic in Rochester, MN. Gene sequencing was performed by next-generation sequencing and Sanger sequencing as previously described [15], at the Mayo Clinic in Rochester, MN.

Results

Histologic evaluation of the subcutaneous soft tissue from both ears showed paucicellular eosinophilic deposits (Fig. 3b) that appeared vaguely fibrillary on low power but also contained numerous small amorphous foci, visible at high power. Congo red stain revealed multiple small Congo red-positive foci (Fig. 3c) with yellow and green birefringence under crossed polarization light microscopy (Fig. 3d). Focal chondroid and bony areas and benign squamous epithelium were also present within the specimen.

LC-MS/MS was performed on the FFPE specimens from both ears, with the Congo red-positive and Congo red-negative areas within the tissue being analyzed separately. The Congo red-positive foci contained abundant cochlin protein spectra, as well as the universal amyloid proteome signature peptides (serum amyloid P component, apolipoprotein A4, and apolipoprotein E) in low abundance. Peptides indicative of a canonical amyloid type were not detected. In contrast, LC-MS/MS performed on the Congo red-negative foci identified abundant cochlin protein spectra but were essentially devoid of the universal amyloid proteome signature peptides (Fig. 4). Immunohistochemistry (IHC) using an anti-cochlin antibody confirmed the presence of cochlin, showing diffuse staining in the deposits (Fig. 5a) with no reactivity in areas of bone, entrapped collagen, or fibrin (Fig. 5b).

A variety of collagens were also detected by LC-MS/MS in both the Congo red-positive and Congo red-negative areas, including collagen alpha-1(I) chain, collagen alpha-2(I) chain, collagen alpha-

3(VI) chain, collagen alpha-1(VI) chain, collagen alpha-1(III) chain, and collagen alpha-2(VI) chain. Of these, collagen alpha-1(I) chain, collagen alpha-2 (I) chains showed the most abundant spectral counts, and were present in greater abundance in the Congo red-positive areas than the Congo red-negative areas. However, the cochlin spectral counts were much higher (Fig. 4).

TEM showed massive deposition of electron-dense material in the extracellular space (Fig. 6a). Similar material was also seen surrounding and within the walls of small vessels (not shown). On higher power, the electron-dense material was composed of densely-packed microfibrils. In some areas, the fibrils were arranged in a swirling pattern and measured 10-24 nm (average 14 nm) in diameter; these areas were reminiscent of amyloid fibrils (compare with much wider and striated collagen fibrils on the right upper corner of Fig. 6b). However, in other areas, the microfibrils were haphazardly oriented, appeared branched, measured 3-7 nm (average 5 nm) in diameter, and were decorated with granular substance consistent with glycosaminoglycans (Fig. 6c); the appearance of the fibrils in these latter areas are similar to those of cochlin deposition previously described in a patient with DFNA9 [16].

Next-generation sequencing of the entire coding region of the *COCH* gene from the patient's blood identified a novel heterozygous germline variant in exon 12, resulting in a non-conservative amino acid substitution of isoleucine to phenylalanine (c.1621A>T, p.I541F) in the vWFA2 domain in the C-terminus of cochlin protein (Fig. 1). This was confirmed by Sanger sequencing, which showed overlapping nucleic acid residues, adenine (A) and thymine (T), indicating heterozygosity for the variant in this position (Fig. 7).

Discussion

Abnormal cochlin deposits are known to occur in the inner and middle ears of patients with DFNA9 deafness as a result of *COCH* mutations [1]. To date, there are no reports of cochlin deposition in the external auditory canal (EAC). Here, we have presented a patient with bilateral EAC stenosis and SNHL (Fig. 2a) caused by cochlin deposits (“cochlinomas”) that show evidence of amyloid formation, associated with a novel variant in the *COCH* gene.

The following findings provided ample evidence that the deposits were composed of cochlin protein: LC-MS/MS demonstrated abundant cochlin peptide spectra throughout the specimens from both ears (Fig. 4); cochlin IHC was positive (Fig. 5a); and TEM showed similarities with previously published EM images of cochlin deposition (Fig. 6c) [16]. Amyloid formation was first suspected due to the presence of numerous Congo red-positive foci (Fig. 3c) with yellow and green birefringence under crossed polarization light microscopy (Fig. 3d), which prompted further workup by protein typing. LC-MS/MS demonstrated a low abundance of universal amyloid proteome signature peptides that were restricted to the Congo red-positive areas in the absence of any protein currently known to form amyloid, raising the possibility of cochlin-derived amyloid formation within the "cochlinomas" (Fig. 4). TEM also corroborated this possibility by revealing swirling fibrils 10-24 nm in diameter (average 14 nm) that were reminiscent of amyloid (Fig. 6b). Furthermore, both next-generation sequencing and Sanger sequencing performed on the patient's blood identified a heterozygous novel variant in the *COCH* gene which encodes cochlin (Figs. 1 and 7).

In diagnostic surgical pathology, Congo red-positive amorphous deposits with yellow and green birefringence under crossed polarization light microscopy elicits a provisional diagnosis of amyloidosis. While Congo red-positive amyloid deposits in the external ear have been reported as a form of primary cutaneous amyloidosis in the auricular concha [17], Congo red reactivity of cochlin protein has not been previously described in the published literature. Rarely, entities other than amyloid may be Congo red-positive, such as DNAJB9 protein in fibrillary glomerulonephritis [18]. In addition, Congo red is a technically challenging stain. Variations in staining conditions, such as solvent type, salt concentration, pH, etc can cause false-positive staining of non-amyloid molecules such as collagen, elastic fibers, and keratin. Cautery artefact can also cause false-positive staining. Variations in staining conditions can cause false-negative Congo red results as well [19]. Therefore, it is imperative that the Congo red staining conditions are correct. If a microscope does not have a strong light source, the characteristic colors of a positive Congo red stain under crossed polarization light microscopy may not be noticeable to the observer, especially if the positive areas are small and/or focal. Lastly, it is important to remember that when examining a Congo red stained slide, the two polarizing filters need to be on either side of the specimen: one

is filter is placed between the light source and the specimen (called the "polarizer"), while the other filter is placed between the specimen and the observer (called the "analyzer") [20].

Once Congo red-positivity is established, it is essential to type the Congo red-positive deposit to help guide the clinical workup and treatment [21]. LC-MS/MS is the most accurate method for typing amyloidosis in light of its high sensitivity and specificity, and is considered the gold standard for amyloid typing [14]. Furthermore, as an unbiased, shotgun proteomics-based assay, it is able to identify rare and potentially previously-unrecognized amyloid types.

In our patient, sequencing of the entire coding region of the *COCH* gene revealed a novel variant (c.1621A>T, p.I541F) in the vWFA2 domain in the protein's C-terminus (Figs. 1 and 7). The immediately adjacent amino acid (position 542) is a cysteine residue, which is critical for the structural and functional integrity of cochlin. Three distinct mutations of this cysteine residue have been reported to cause DFNA9 deafness disorder. It has been shown that changes at residue C542 disrupt cochlin intramolecular disulfide bonding [22]. It is likely that in our case, the non-conservative amino acid change in the immediately adjacent (position 541) isoleucine (an aliphatic amino acid residue) to phenylalanine (a bulky aromatic residue) also interferes with proper protein folding and disrupts the overall tertiary structure of cochlin, possibly causing amyloid-like structural changes. Furthermore, variants in the vWFA2 domain may result in abnormal collagen binding with potential disruption of normal extracellular matrix composition.

Given the sensorineural nature of the patient's hearing loss, it is possible that she has undetected deposits in the inner and middle ears similar to other patients with DFNA9, but uniquely with extension into the external ear canal. It is unknown whether the patient's hearing-impaired family members share the same genetic variant. Also, the significance of the patient's and her family's increased intraorbital pressures is unknown. However, further exploration of these uncertainties is not feasible at this time.

Conclusion

In summary, we have described the first case of bilateral external auditory canal deposits consisting of cochlin protein with numerous amyloid-like deposits, in a patient with sensorineural hearing loss. The patient has a novel variant in her *COCH* gene that corresponds to the vWFA2 domain in cochlin protein's C-terminus (heterozygous c.1621A>T, p.I541F). Our case study illustrates a new manifestation of cochlin, and our evidence from Congo red stain, immunohistochemical stain, LC-MS/MS, and electron microscopy raise the possibility of previously undescribed cochlin-derived amyloid formation. Further studies are needed to explore the possible disease mechanisms implied by this novel *COCH* variant, its corresponding alterations to cochlin's structure and functions, as well as its microscopic and clinical manifestations.

Our report highlights the need for thorough characterization of aggregative tissue findings in the practice of diagnostic surgical pathology. In our case, the specimen was paucicellular and there was an absence of cellular clues such as plasma cells or multinucleated histiocytes, thereby appearing rather "plain" at first glance. Given its fibrillary features at low power, it can potentially be dismissed as sclerosis or fibrosis. The Congo red stain was positive in multiple small foci, and was not diffuse. However, our report demonstrates that aggregative deposits from anywhere in the ear, even with small amorphous foci, warrant further work-up for the possibility of "cochlinoma," particularly if the patient has hearing impairment. The mindful pathologist incorporates the burgeoning array of ancillary testing modalities into his or her diagnostic algorithm to identify diseases "hiding in plain sight."

References

1. Robertson NG, Cremers CW, Huygen PL, Ikezono T, Krastins B, Kremer H et al. Cochlin immunostaining of inner ear pathologic deposits and proteomic analysis in DFNA9 deafness and vestibular dysfunction. Human molecular genetics. 2006;15(7):1071-85. doi:10.1093/hmg/ddl022.

2. Ikezono T, Omori A, Ichinose S, Pawankar R, Watanabe A, Yagi T. Identification of the protein product of the Coch gene (hereditary deafness gene) as the major component of bovine inner ear protein. Biochimica et biophysica acta. 2001;1535(3):258-65.

3. Robertson NG, O'Malley JT, Ong CA, Giersch AB, Shen J, Stankovic KM et al. Cochlin in normal middle ear and abnormal middle ear deposits in DFNA9 and Coch (G88E/G88E) mice.

Journal of the Association for Research in Otolaryngology : JARO. 2014;15(6):961-74. doi:10.1007/s10162-014-0481-9.

4. Robertson NG, Lu L, Heller S, Merchant SN, Eavey RD, McKenna M et al. Mutations in a novel cochlear gene cause DFNA9, a human nonsyndromic deafness with vestibular dysfunction. Nature genetics. 1998;20(3):299-303. doi:10.1038/3118.

5. Khetarpal U, Schuknecht HF, Gacek RR, Holmes LB. Autosomal dominant sensorineural hearing loss. Pedigrees, audiologic findings, and temporal bone findings in two kindreds. Archives of otolaryngology--head & neck surgery. 1991;117(9):1032-42.

6. McCall AA, Linthicum FH, Jr., O'Malley JT, Adams JC, Merchant SN, Bassim MK et al. Extralabyrinthine manifestations of DFNA9. Journal of the Association for Research in Otolaryngology : JARO. 2011;12(2):141-9. doi:10.1007/s10162-010-0245-0.

7. Robertson NG, Skvorak AB, Yin Y, Weremowicz S, Johnson KR, Kovatch KA et al. Mapping and characterization of a novel cochlear gene in human and in mouse: a positional candidate gene for a deafness disorder, DFNA9. Genomics. 1997;46(3):345-54. doi:10.1006/geno.1997.5067.

8. Picciani R, Desai K, Guduric-Fuchs J, Cogliati T, Morton CC, Bhattacharya SK. Cochlin in the eye: functional implications. Progress in retinal and eye research. 2007;26(5):453-69. doi:10.1016/j.preteyeres.2007.06.002.

9. Py BF, Gonzalez SF, Long K, Kim MS, Kim YA, Zhu H et al. Cochlin produced by follicular dendritic cells promotes antibacterial innate immunity. Immunity. 2013;38(5):1063-72. doi:10.1016/j.immuni.2013.01.015.

10. Nystrom A, Bornert O, Kuhl T, Gretzmeier C, Thriene K, Dengjel J et al. Impaired lymphoid extracellular matrix impedes antibacterial immunity in epidermolysis bullosa. Proceedings of the National Academy of Sciences of the United States of America. 2018;115(4):E705-e14. doi:10.1073/pnas.1709111115.

11. Jung J, Yoo JE, Choe YH, Park SC, Lee HJ, Lee HJ et al. Cleaved Cochlin Sequesters Pseudomonas aeruginosa and Activates Innate Immunity in the Inner Ear. Cell host & microbe. 2019;25(4):513-25.e6. doi:10.1016/j.chom.2019.02.001.

12. Bae SH, Robertson NG, Cho HJ, Morton CC, Jung DJ, Baek JI et al. Identification of pathogenic mechanisms of COCH mutations, abolished cochlin secretion, and intracellular aggregate formation: genotype-phenotype correlations in DFNA9 deafness and vestibular disorder. Human mutation. 2014;35(12):1506-13. doi:10.1002/humu.22701.

13. Cho HJ, Park HJ, Trexler M, Venselaar H, Lee KY, Robertson NG et al. A novel COCH mutation associated with autosomal dominant nonsyndromic hearing loss disrupts the structural stability of the vWFA2 domain. Journal of molecular medicine (Berlin, Germany). 2012;90(11):1321-31. doi:10.1007/s00109-012-0911-2.

14. Vrana JA, Gamez JD, Madden BJ, Theis JD, Bergen HR, 3rd, Dogan A. Classification of amyloidosis by laser microdissection and mass spectrometry-based proteomic analysis in clinical biopsy specimens. Blood. 2009;114(24):4957-9. doi:10.1182/blood-2009-07-230722.

15. Baudhuin LM, Lagerstedt SA, Klee EW, Fadra N, Oglesbee D, Ferber MJ. Confirming Variants in Next-Generation Sequencing Panel Testing by Sanger Sequencing. The Journal of molecular diagnostics : JMD. 2015;17(4):456-61. doi:10.1016/j.jmoldx.2015.03.004.

16. Khetarpal U. DFNA9 is a progressive audiovestibular dysfunction with a microfibrillar deposit in the inner ear. The Laryngoscope. 2000;110(8):1379-84. doi:10.1097/00005537-200008000-00030.

17. Abuawad YG, Uchiyama J, Kakizaki P, Valente NYS. Primary cutaneous amyloidosis of the auricular concha - case report. Anais brasileiros de dermatologia. 2017;92(3):433-4. doi:10.1590/abd1806-4841.20175864.

18. Alexander MP, Dasari S, Vrana JA, Riopel J, Valeri AM, Markowitz GS et al. Congophilic Fibrillary Glomerulonephritis: A Case Series. American journal of kidney diseases : the official journal of the National Kidney Foundation. 2018;72(3):325-36. doi:10.1053/j.ajkd.2018.03.017.

19. Yakupova EI, Bobyleva LG, Vikhlyantsev IM, Bobylev AG. Congo Red and amyloids: history and relationship. Bioscience reports. 2019;39(1). doi:10.1042/bsr20181415.

20. Howie AJ, Brewer DB. Optical properties of amyloid stained by Congo red: history and mechanisms. Micron (Oxford, England : 1993). 2009;40(3):285-301. doi:10.1016/j.micron.2008.10.002.

21. Rocken C, Sletten K. Amyloid in surgical pathology. Virchows Archiv : an international journal of pathology. 2003;443(1):3-16. doi:10.1007/s00428-003-0834-y.

22. Street VA, Kallman JC, Robertson NG, Kuo SF, Morton CC, Phillips JO. A novel DFNA9 mutation in the vWFA2 domain of COCH alters a conserved cysteine residue and intrachain disulfide bond formation resulting in progressive hearing loss and site-specific vestibular and central oculomotor dysfunction. American journal of medical genetics Part A. 2005;139a(2):86-95. doi:10.1002/ajmg.a.30980.

Figure Legends

Fig. 1 Schematic representation of *COCH* gene, encoding cochlin, showing the signal peptide (SP) for secretion, followed by the LCCL domain, and intervening domain (ivd1) followed by two vWFA-like domains separated by ivd2. Positions of previously known pathogenic variants (27 missense and 2 in-frame deletions) are indicated in black. The novel I541F variant (the subject of our current report) is shown in red and with an asterisk. Positions of all cysteine residues (C),

which are critical for disulfide bond formation and the structural integrity of the protein, are indicated.

Fig. 2 (**a**) A presurgical view of the left external auditory canal with speculum in place, revealing significant soft tissue stenosis with normal overlying skin. (**b**) Post-surgically, a wide view to the intact tympanic membrane was appreciated.

Fig. 3 (**a**) During the meatoplasty and bony canaloplasty procedure, incisions were created, anterior and posterior flaps were raised, well-encapsulated tan brown soft tissue was detected beneath the skin (white arrow), and all abnormal subcutaneous soft tissue was excised. (**b**) Histologic examination of the subcutaneous soft tissue revealed paucicellular eosinophilic deposits with numerous small amorphous foci (H&E stain, 10x). (**c**) There were multiple Congo red-positive foci (Congo red stain, 10x). (**d**) Yellow and green birefringence under crossed polarization light microscopy was observed (Congo red stain, 10x).

Fig. 4 Liquid chromatography tandem mass spectrometry (LC-MS/MS) performed on both the Congo red-positive (CR +ve) (samples 1 & 2) and Congo red-negative (CR -ve) (samples 3 & 4) areas identified abundant cochlin protein spectra throughout, as well as a low abundance of universal amyloid proteome signature peptides in the Congo red-positive areas but not in the Congo red-negative areas. Peptides indicative of a canonical amyloid type were not detected.

Fig. 5 (**a**) Immunohistochemistry for cochlin protein showed diffuse staining in the amorphous deposits, with no reactivity in bone, entrapped stroma, and fibrin (arrows). (**b**) Corresponding hematoxylin & eosin stained section.

Fig. 6 Transmission electron microscopy. (**a**) There was massive deposition of electron-dense material in the extracellular space (original magnification, x4800). (**b**) On higher power, the electron-dense material was composed of densely packed microfibrils. In some areas, the fibrils were arranged in a swirling pattern, measured 10-24 nm (average 14 nm) in diameter, and were reminiscent of amyloid fibrils (compare with much larger and striated collagen fibrils on the right upper corner of the image) (x23,000). (**c**) In other areas, microfibrils were haphazardly oriented, appeared branched, measured 3-7 nm (average 5 nm) in diameter, and were decorated with granular substance consistent with glycosaminoglycans (x49,000). They are similar to the fibrils previously described in a patient with DFNA9.

Fig. 7 (**a**) Sanger sequencing traces, highlighting (red arrow) the c.1612A>T (p.Ile541Phe) variant in *COCH.* Sequencing was performed on both a control specimen and our patient in the forward

direction (represented on the top) and in the reverse direction (on the bottom). The sequence traces show overlapping nucleic acid residues, adenine (A) and thymine (T), in the forward direction, indicating heterozygosity for the variant in this position. (**b**) Cochlin amino acid sequence, showing the altered isoleucine (I) residue, highlighted in green.

Figure 1

Click here to access/download;Figure;Figure 1 - COCH gene schematic.png

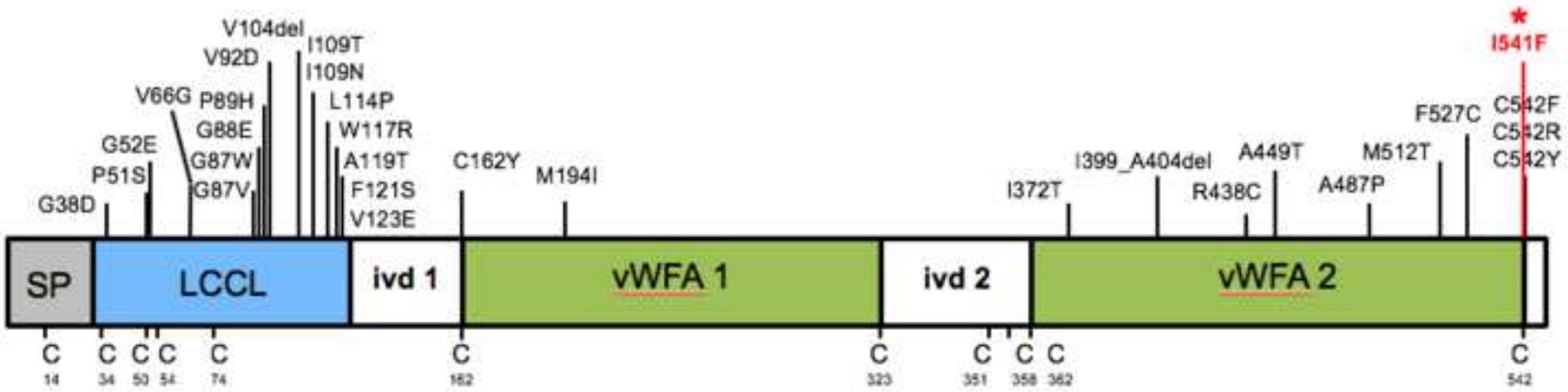

Figure 2A

Click here to access/download;Figure;Figure 2A - EACStenosis.jpg

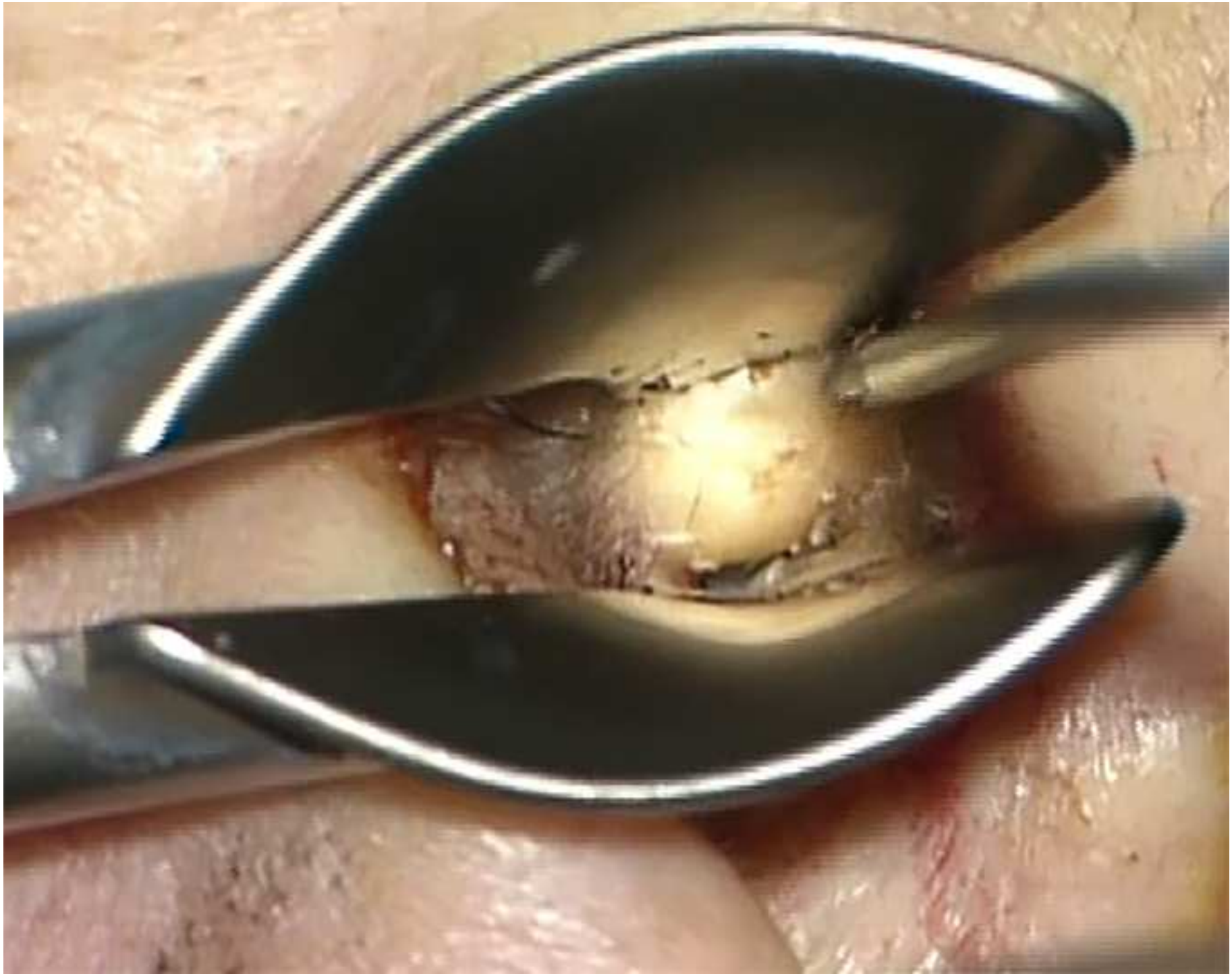

Figure 2B

Click here to access/download;Figure;Figure 2B - OpenToTM.jpg

Figure 3A

Click here to access/download;Figure;Figure 3A - EACSubcutaneousTissue.jpg

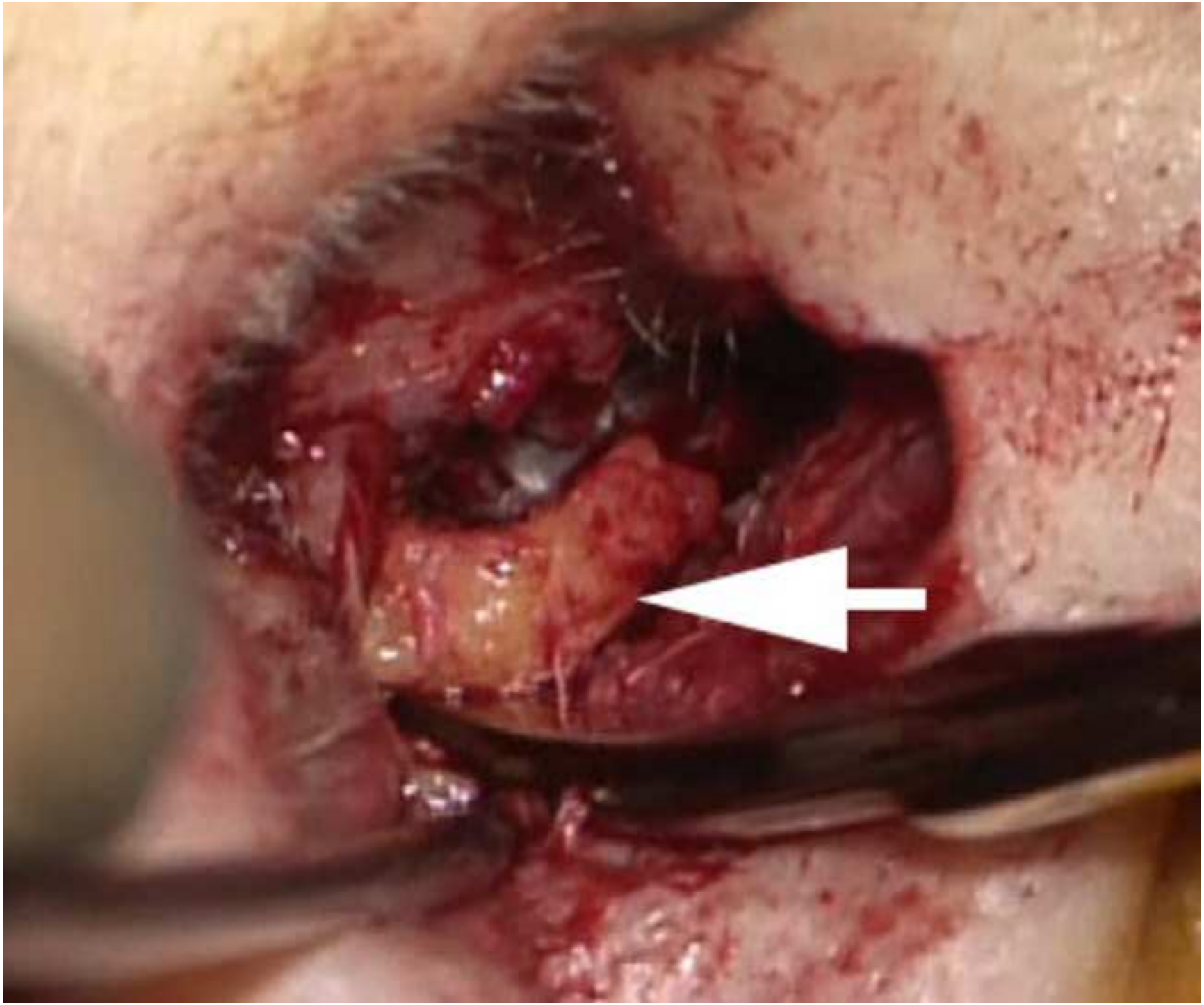

Figure 3B

Click here to access/download;Figure;Figure 3B - H&E 10x.tif

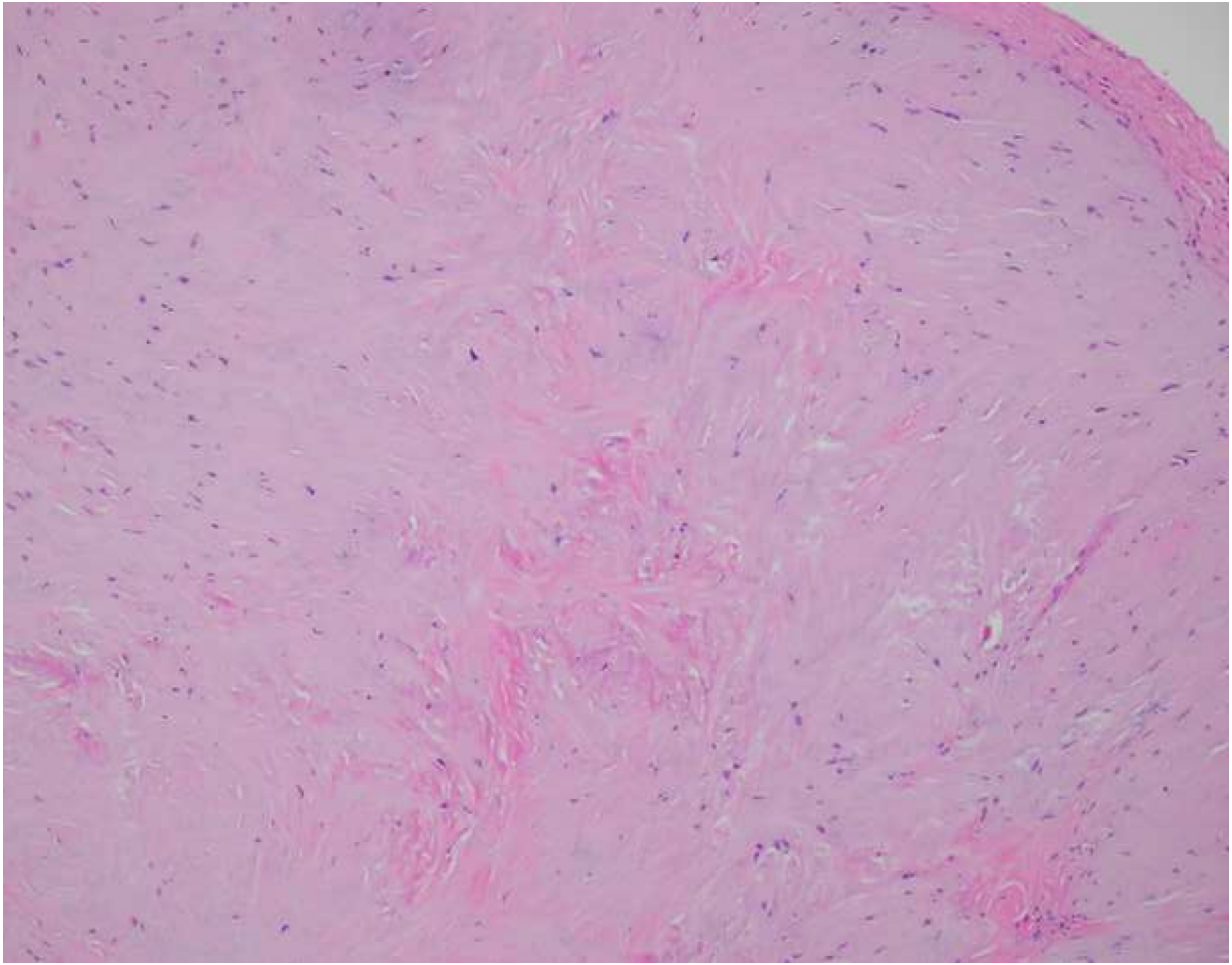

Figure 3C

Click here to access/download;Figure;Figure 3C - Congored 10x.tif

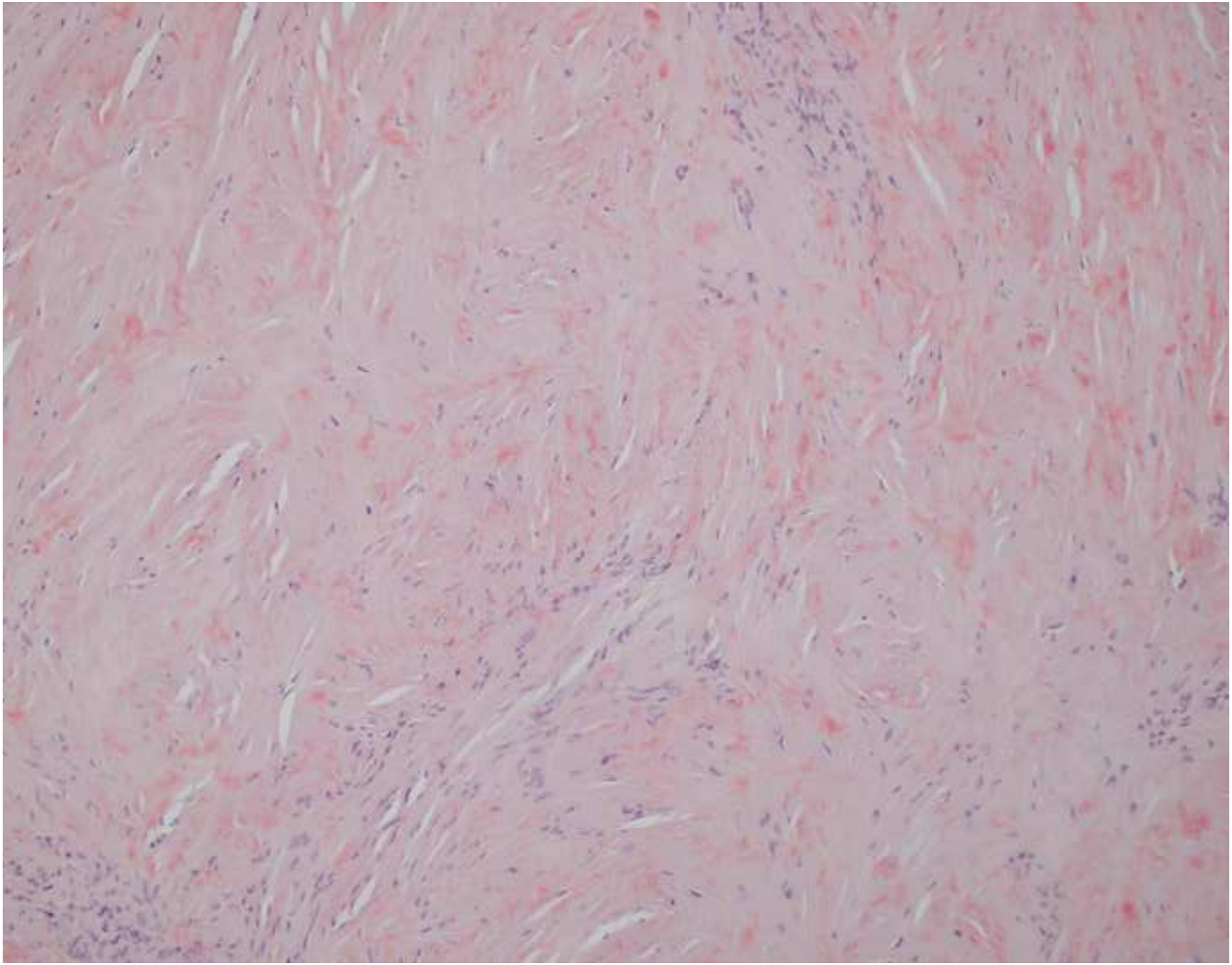

Figure 3D

Click here to access/download;Figure;Figure 3D - Congored polarized 10x.tif

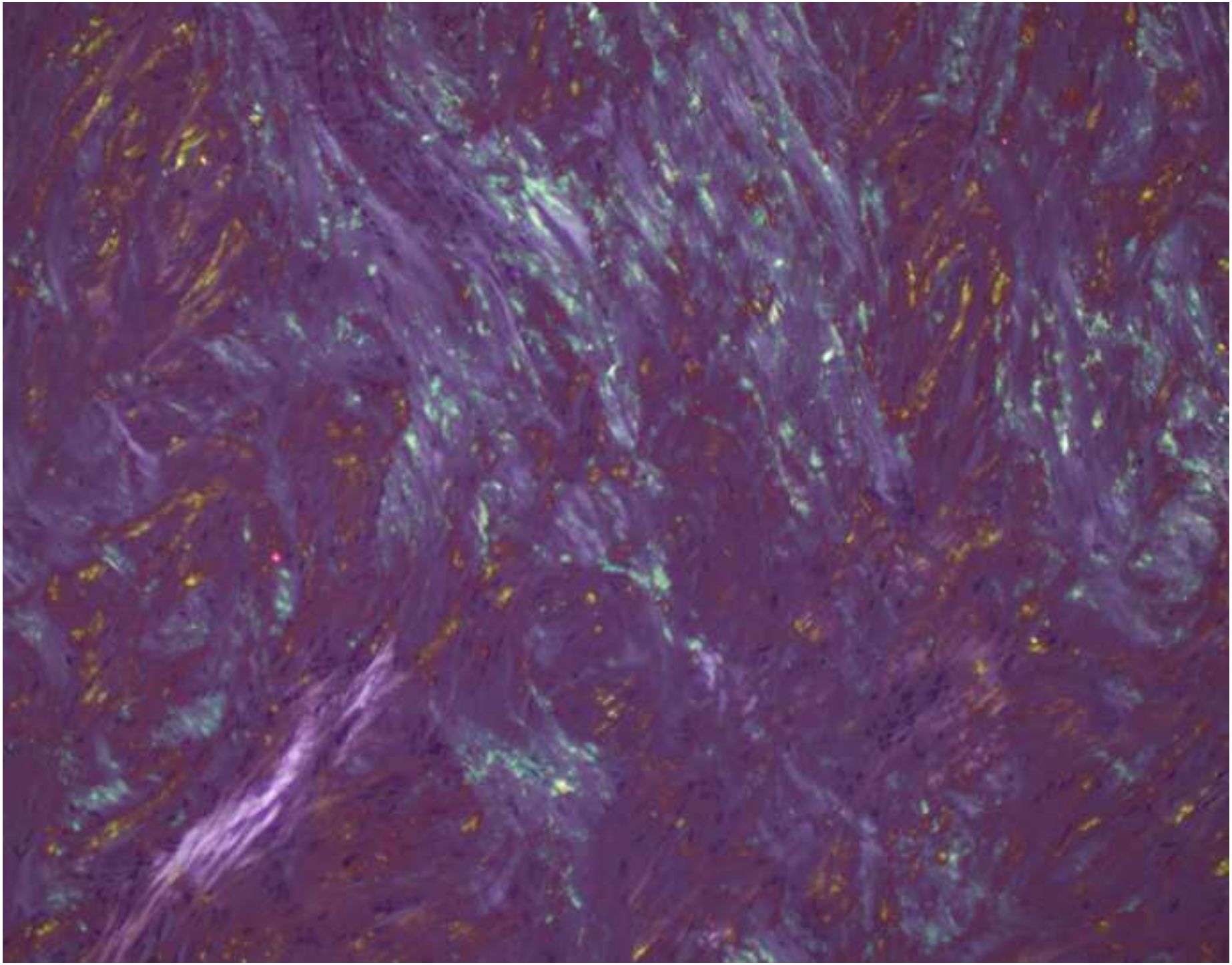

Figure 4

Click here to access/download;Figure;Figure 4 - mass spec table.tif

Probability Legend:

- over 95%
- 80% to 94%
- 50% to 79%
- 20% to 49%
- 0% to 19%

Bio View:
Identified Proteins (59/60)
Including 2 Decoys

#	Visible?	Starred?		Accession Number	Molecular Weight	Protein Grouping Ambiguity	CR +ve		CR -ve Dense Deposit	
							Sample 1	Sample 2	Sample 3	Sample 4
1	☑	★	Cochlin	COCH_HUMAN	59 kDa		348	346	393	465
2	☑	★	Apolipoprotein A-IV	APOA4_HUMAN	45 kDa		20	26	3	
3	☑	★	Serum amyloid P-component	SAMP_HUMAN	25 kDa		16	14	2	2
4	☑	★	Apolipoprotein E	APOE_HUMAN	36 kDa		16	17		
5	☑	☆	Vimentin	VIME_HUMAN	54 kDa	★	104	80	71	186
6	☑	☆	Serum albumin	ALBU_HUMAN	69 kDa		97	84	113	59
7	☑	☆	Collagen alpha-2(I) chain	CO1A2_HUMAN	129 kDa		121	102	54	45
8	☑	☆	Hemoglobin subunit beta	HBB_HUMAN	16 kDa	★	101	66	93	79
9	☑	☆	Collagen alpha-1(I) chain	CO1A1_HUMAN	139 kDa		118	100	41	35
10	☑	☆	Hemoglobin subunit alpha	HBA_HUMAN	15 kDa		102	64	80	64

Figure 5A

Click here to access/download;Figure;Figure 5A - cochlin IHC.tif

Figure 5B

Click here to access/download;Figure;Figure 5B - corresponding cochlin HE.tif

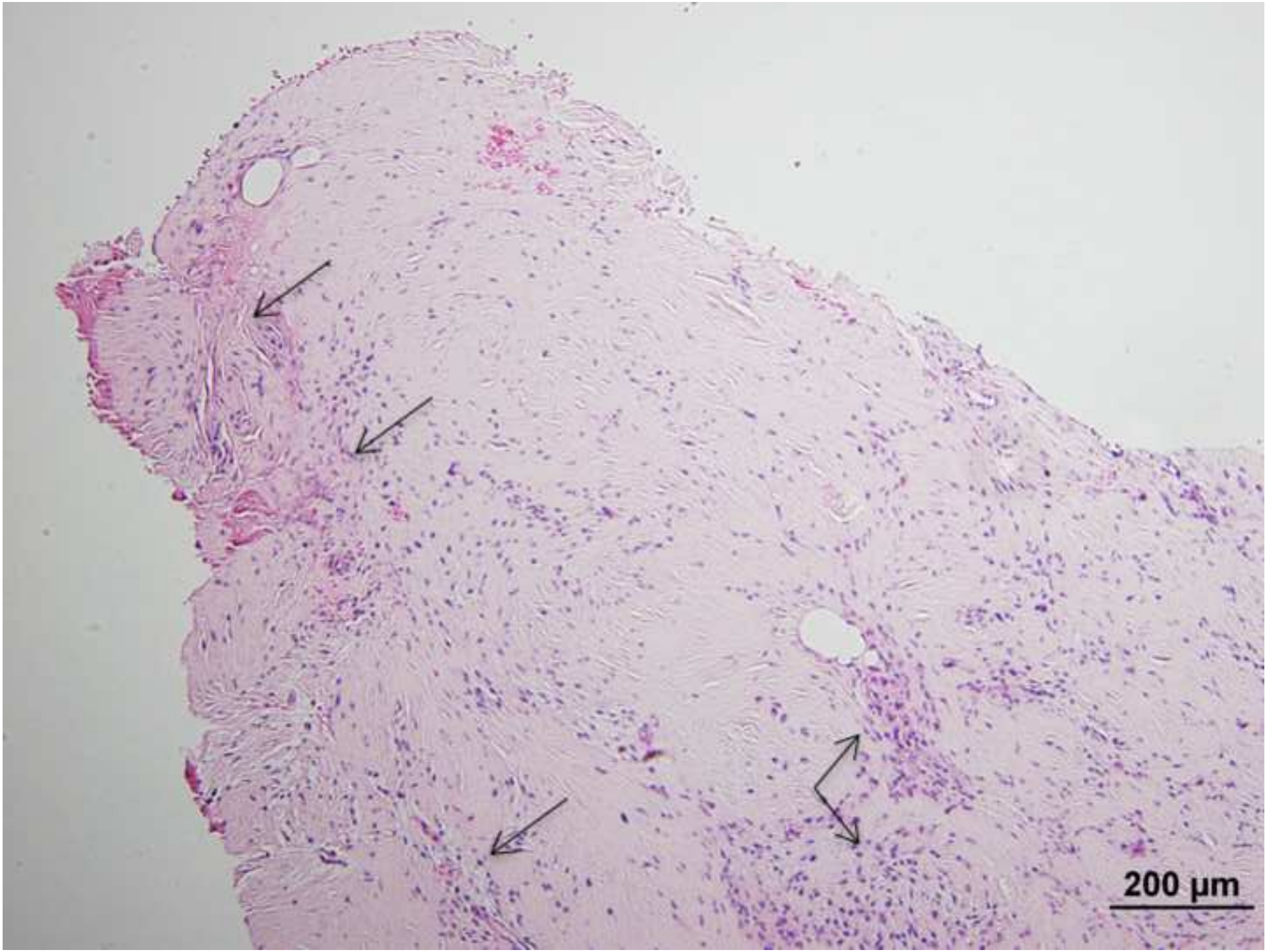

Figure 6A

Click here to access/download;Figure;Figure 6A - EM massive deposition.tif

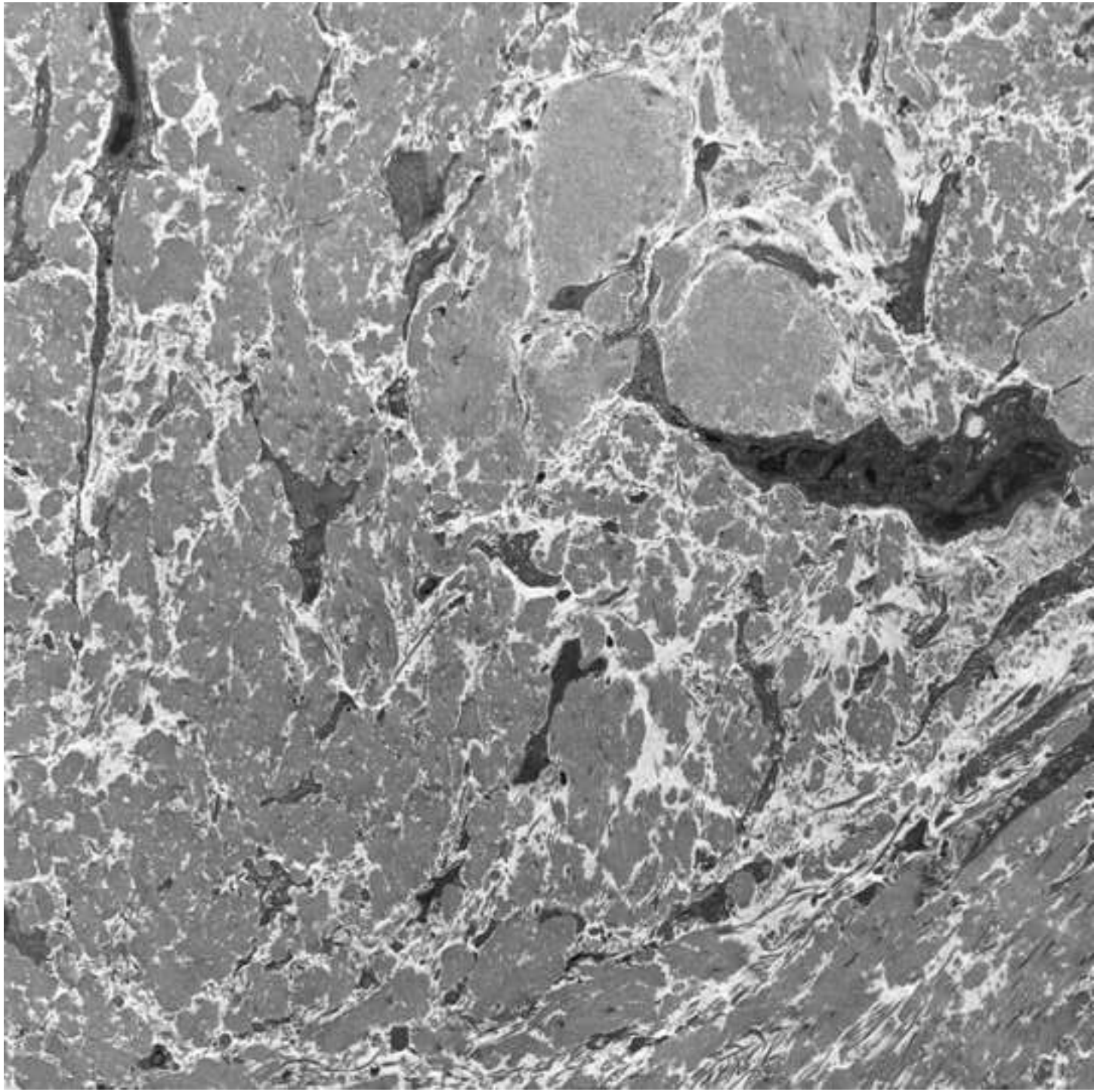

Figure 6B

Click here to access/download;Figure;Figure 6B - EM swirling 14 nm.tif

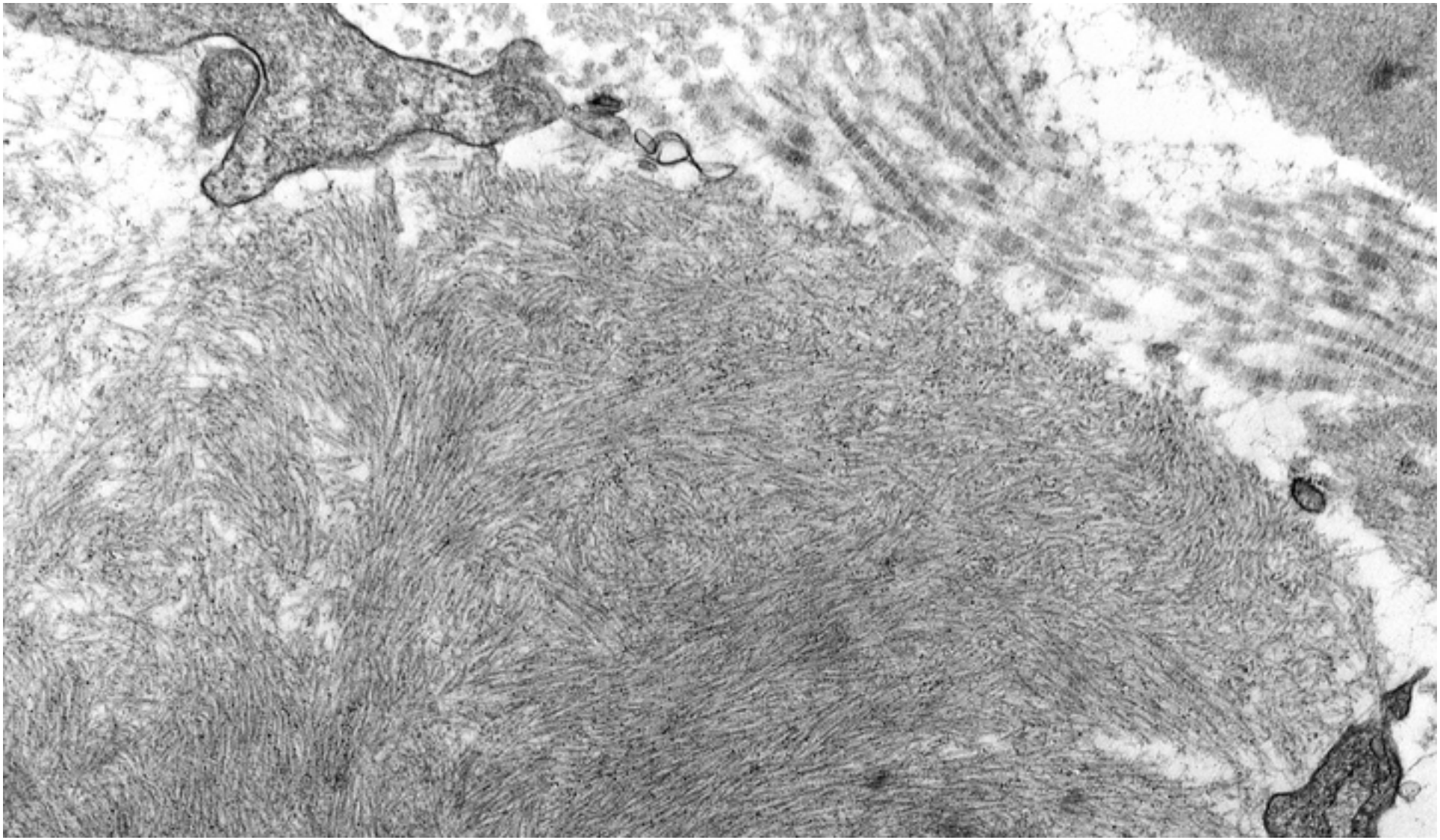

Figure 6C

Click here to access/download;Figure;Figure 6C - EM branched granular 5 nm.tif

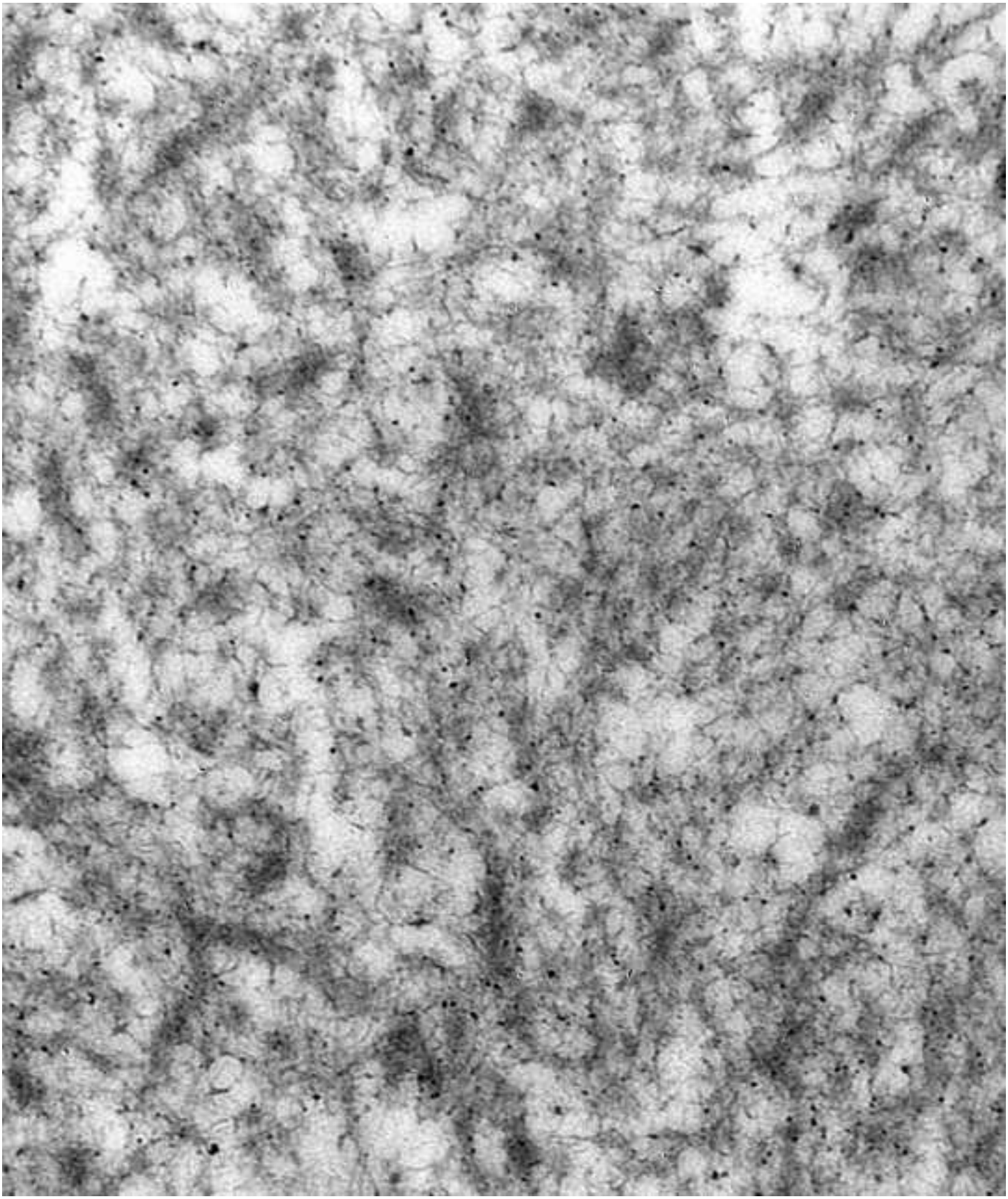

Figure 7A

Click here to access/download;Figure;Figure 7A Sanger Sequence Trace.tif

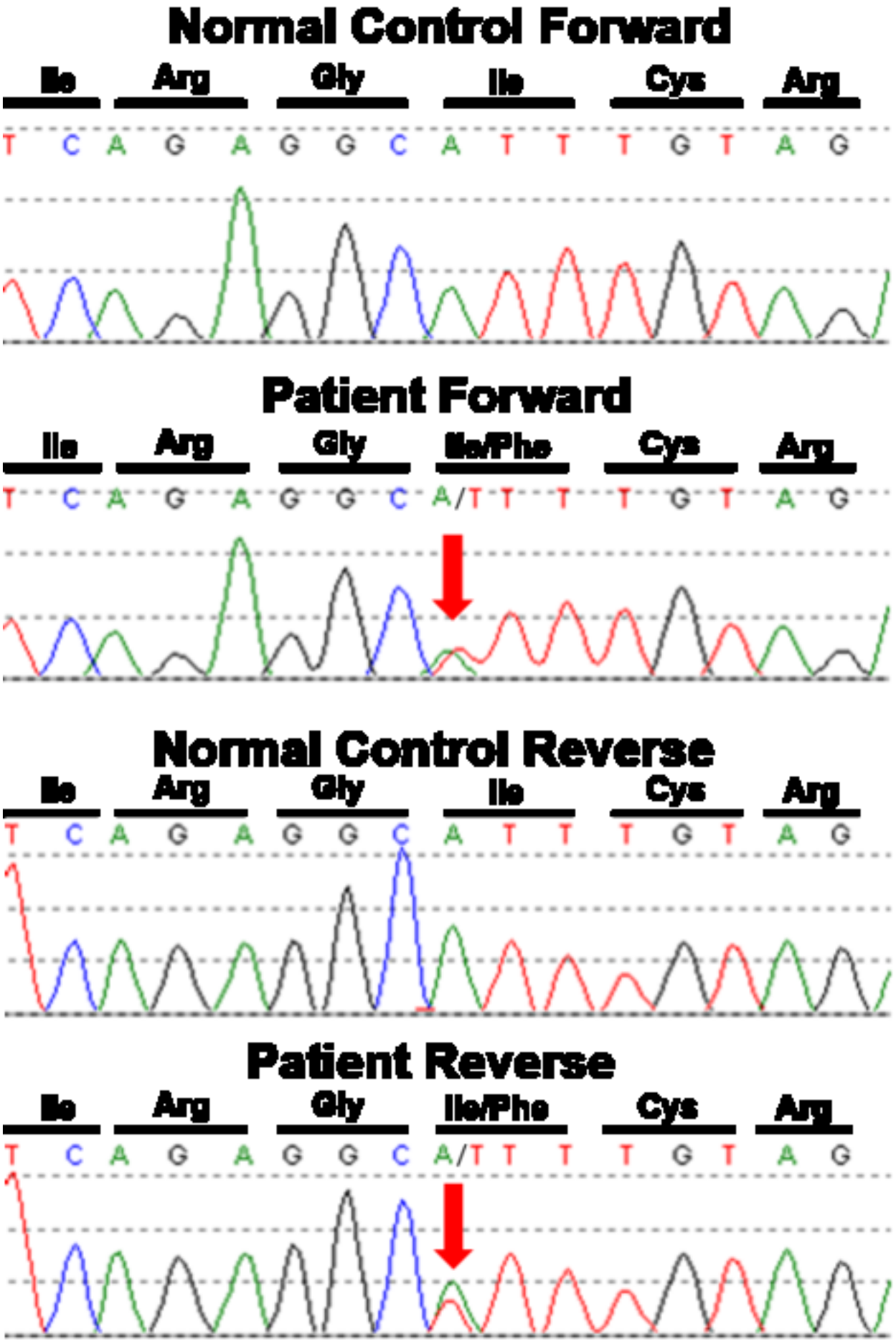

Figure 7B

Cochlin (550 aa):

MSAAWIPALGLGVCLLLLPGPAGSEGAAPIAITCFTRGLDIRKEKADVLCPGGCPLEEFSVYGNIVYASV
SSICGAAVHRGVISNSGGPVRVYSLPGRENYSSVDANGIQSQMLSRWSASFTVTKGKSSTQEATGQAVST
AHPPTGKRLKKTPEKKTGNKDCKADIAFLIDGSFNIGQRRFNLQKNFVGKVALMLGIGTEGPHVGLVQAS
EHPKIEFYLKNFTSAKDVLFAIKEVGFRGGNSNTGKALKHTAQKFFTVDAGVRKGIPKVVVVFIDGWPSD
DIEEAGIVAREFGVNVFIVSVAKPIPEELGMVQDVTFVDKAVCRNNGFFSYHMPNWFGTTKYVKPLVQKL
CTHEQMMCSKTCYNSVNIAFLIDGSSSVGDSNFRLMLEFVSNIAKTFEISDIGAKIAAVQFTYDQRTEFS
FTDYSTKENVLAVIRNIRYMSGGTATGDAISFTVRNVFGPIRESPNKNFLVIVTDGQSYDDVQGPAAAAH
DAGITIFSVGVAWAPLDDLKDMASKPKESHAFFTREFTGLEPIVSDVIRGICRDFLESQQ